

A 1 MHz Boost DC-DC Converter with Turn on ZCS Capability to Reduce EMI

1st Hiroki Yoshioka
Kyoto Institute of Technology
Kyoto, Japan
hyoshioka@vlsi.es.kit.ac.jp

2nd Jun Furuta
Kyoto Institute of Technology
Kyoto, Japan
furuta@vlsi.es.kit.ac.jp

3rd Kazutoshi Kobayashi
Kyoto Institute of Technology
Kyoto, Japan
kazutoshi.kobayashi@kit.ac.jp

Abstract—This paper proposes a boost DC-DC converter with turn-on zero current switching (ZCS) capability to suppress electromagnetic interference (EMI) generated from an output diode. When a switching component turn on, reverse current flows from the output diode. In SiC-SBD, reverse recovery time is very short and conduction loss is small, but noise is increased by switching speed over MHz. By operating in discontinuous current mode, noise at turn-on can be reduced. However, at high frequency over MHz, the conduction loss increases because peak current flowing through the switching component and inductor increases. Radiated EMI of the boost DC-DC converter is reduced by the ZCS soft switching at turn on operating in the continuous current mode. Measurement results of EMI of the ZCS DC-DC converter were presented to confirm EMI suppression from the ZCS operation.

Index Terms—Soft switching, Electromagnetic interference, DC-DC converter, Silicon Carbide, Schottky diodes, Switches.

I. INTRODUCTION

By wide gap semiconductors such as GaN and SiC, power conversion circuits have become possible to operate at higher frequency over MHz [1], [2]. They can be downsized by replacing passive components with smaller ones owing to the high frequency operation [3]. Recently, boost DC-DC converters are used in electric vehicles [4], and they need to be made smaller and more efficient.

Reverse recovery current is a major problem for diodes used in boosted DC-DC converter [5], [6]. Reverse recovery current flows to the switching component and induces power loss on a conventional boost dc-dc converter (Fig. 1) [7]. If reverse recovery time is long such as Si diode, switching frequency is limited. SiC-SBD has shorter reverse recovery time, so power loss is smaller than Si-FRD [8]. Although these semiconductors enable high-frequency operation, high frequency switching suffers from ringing caused by parasitic inductance and capacitance of switching components and wires. In particular, high di/dt due to the reverse recovery time of SiC-SBD causes a very large ringing at turn-on [9], [10]. Figures 2 and 3 show V_{DS} and V_{GS} waveforms when Si-FRD or SiC-SBD is used as an output diode of a boost DC-DC converter in Fig. 1. We use same measurement conditions (Voltage, Duty rate, Measurement board etc.) except for diode. In Fig. 3, a large ringing is observed at turn on. This ringing leads to increase radiated EMI. We have to need to measure ringing at turn on.

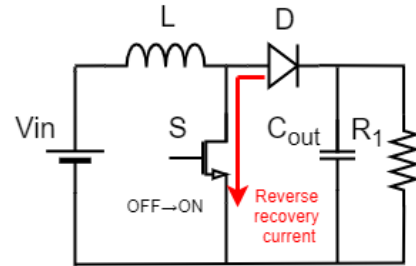


Fig. 1: Reverse recovery current at conventional Boost dc-dc converter

One way to reduce EMI is the soft switching technology [11], [12]. However, if all switching component is achieved soft switching, it needs many additional components [13]. That cause increasing conduction loss and circuit size. The circuit shown in Fig. 4 is a boost DC-DC converter, which has ZCS capability at only turn-on (named CIR 1). The circuit in Fig. 4 is a structure which removed capacitor C1 from soft switching boost dc-dc converter in Fig 5 [14]. Although switching loss at turn off is increased by removing C1, CIR 1 can decrease conduction loss with some additional components and it is easy to control. When a GaN HEMT is used as a switching component, switching loss at turn off becomes small [15]. We compare CIR 1 and 2 in terms of conversion efficiency and radiated EMI.

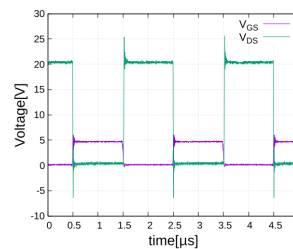


Fig. 2: Waveform of V_{GS} - V_{DS} (Si FRD)

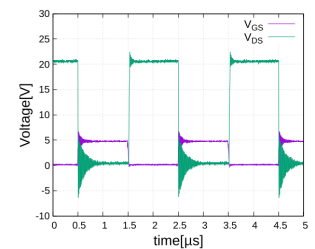


Fig. 3: Waveform of V_{GS} - V_{DS} (SiC SBD)

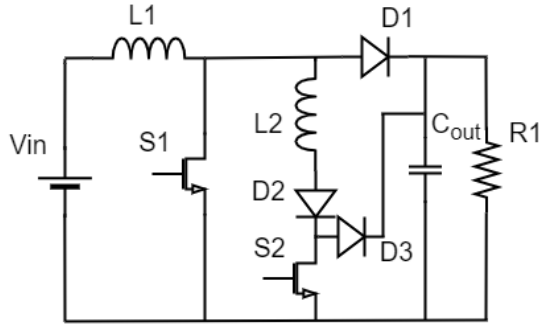


Fig. 4: Proposed circuit (CIR 1)

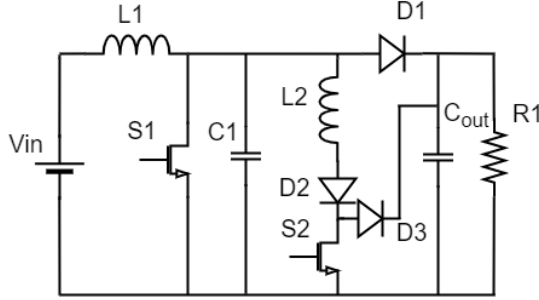


Fig. 5: Soft switching boost dc-dc converter (CIR 2)

II. OPERATION OF PROPOSED BOOST DC-DC CONVERTER

Fig. 4 shows a proposed boost dc-dc converter (named as CIR 1). It has additional components compared with the conventional boost dc-dc converter in Fig. 1, inductor L2, Diodes D2 and D3 and auxiliary switching component S2. In the circuit (CIR 2) proposed in previous research paper [14], as shown in Fig. 5, a resonant capacitor C1 is further added. A saturable reactor is required between L2 and D2 to prevent S1 and L2 from resonating. Inductance of L2 should be sufficiently smaller than L1. Fig. 6 shows procedure of the proposed circuit. Fig. 7 shows waveforms of the proposed circuit. There are four operation modes within one switching cycle.

mode 1 (t_0-t_1) At t_0 , S2 is turned on. Current flowing through L2 linearly increases and current flowing through D1 linearly decreases. S2 is turned on with ZCS (Zero current switching). At t_1 , current flowing through L1 and L2 are equivalent because inductance of L2 is smaller than that of L1. The period t_{0-1} (Turn-on time of S2 $t_{on(S2)}$) is given by

$$t_{0-1} = t_{on(S2)} = \frac{I_{in}L_2}{V_{out}} \quad (1)$$

mode 2 (t_1-t_2) S1 is turned on, and S2 is turned off. Current flowing through D3 linearly decreases until it reaches zero at t_2 . Current flowing through S1 linearly increases. S2 is turned off with hard switching, S1 is turned on with ZCS.

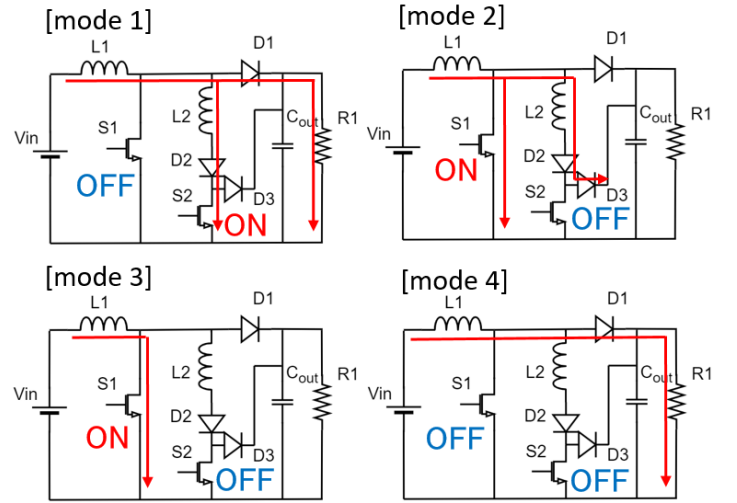


Fig. 6: Operation of CIR 1

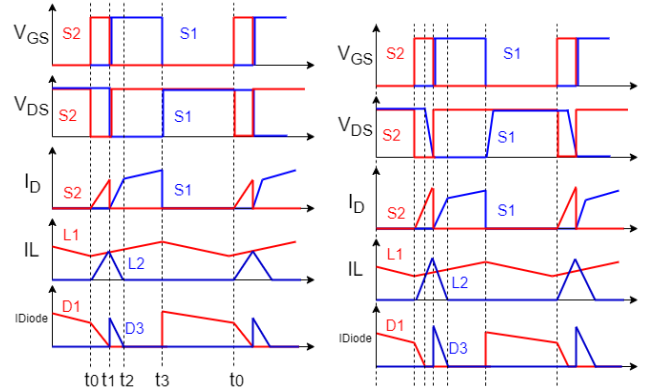


Fig. 7: Waveform of CIR 1 Fig. 8: Waveform of CIR 2

mode 3 (t_2-t_3) Current flows through S1 only and L1 stores energy as same as the conventional boost dc-dc circuit. At t_3 , S1 is turned off with hard switching.

mode 4 (t_3-t_0) This interval is identical to the freewheeling stage of the conventional boost dc-dc converter. Transfer the energy stored in the L1 to the load resistance.

Fig. 8 shows an operating waveform of CIR 2 [14]. The operation is almost same as the proposed circuit. In CIR 2, the resonant capacitor C1 is discharged after the current flowing through L2 becomes equal to the current flowing through L1. The charge of C1 becomes zero, so S1 is turned off with ZVS. Turn-on time of S2 is given by :

$$t_{on(S2)} = \frac{I_{in}L_2}{V_{out}} + \frac{\pi}{2} \sqrt{L_2C_1} \quad (2)$$

Conduction loss of L2, S2, S2 and D3 increases because the on time of S2 is longer than in the proposed circuit.

TABLE I: Major components in the circuit

Component	value
Switches S1, S2	IGO60R070D1AUMA1 (from Infineon)
Gate driver	SI8275GB-IS1 (from Silicon Labs)
Diodes D1 D2 D3	SCS310AJTLL (from Rohm)
Inductor L1	47 μ H, $R_{on} = 26$ m Ω
Inductor L2	3.3 μ H, $R_{on} = 5.76$ m Ω
Output capacitor C_{out}	1 μ F
Resonance capacitor C1	1 nF

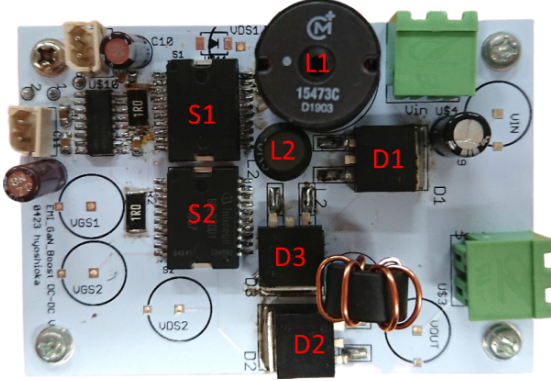


Fig. 9: Measurement board

III. MEASUREMENT RESULTS

Efficiency and radiated EMI are measured in the proposed circuit (CIR 1), the proposed circuit in the previous paper [14] (CIR 2), and the conventional circuit. Table I shows components used for the measurements. Radiated EMI measurement conditions are as follows; Operating frequency of 1 MHz, input voltage of 25 V, output voltage of 50 V, output power of 25W. Since it is difficult to cool the load resistance, the measurement is made at low power. We measured radiated EMI in our 3 m method anechoic chamber. Fig. 9 shows a measurement board. The same board is used for the all measurements. Gate voltage for the GaN HEMT is set at 5 V. Analog Discovery 2 (from Digilent Inc.) is used as a function generator to send control signals to the gate driver.

Fig. 10 shows a radiated EMI measurement environment in the anechoic chamber. The measurement board is placed on the table and all experimental equipment is put under it. The experimental equipment consists of a power supply equipment, an Analog discovery 2, and a PC. They are covered with a shielding fabric (from TAIYO WIRE CLOTH CO.). The measurement result of radiated EMI by the experimental equipment is shown in Fig. 11.

A. Waveform of V_{DS} and radiated EMI

Figures 12 and 13 show measurement results of waveforms of V_{DS} and radiated EMI for each circuit.

1) *Conventional circuit*: In Fig. 12(a), V_{DS} of the conventional circuit contains large ringing at turn on. It is caused by high di/dt reverse recovery current of SiC-SBD. This ringing at 75MHz increases radiated EMI around 75MHz in

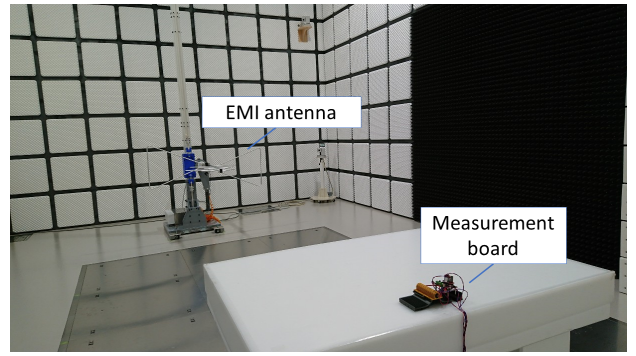


Fig. 10: Radiated EMI measurement environment

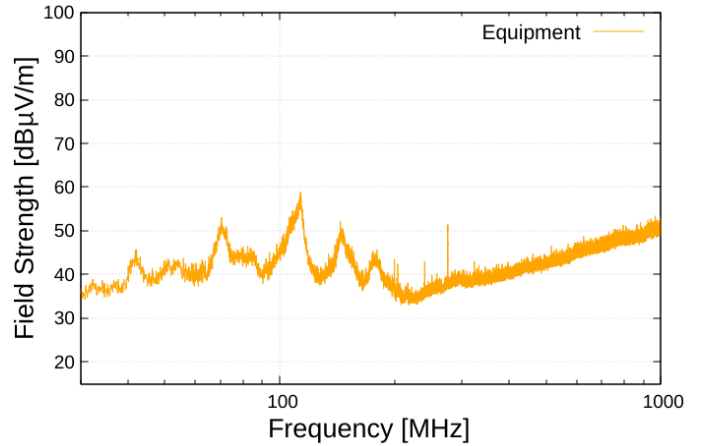


Fig. 11: Measurement result of radiated EMI by equipment

Fig. 13(a). Another EMI peak at 147 MHz appears as the 2nd harmonic by 72 MHz radiated EMI. We confirmed that the reverse recovery current of SiC-SBD increases the radiated EMI in the conventional circuit.

2) *Proposed circuit (CIR 1)*: As shown in Fig. 12(b), there is a ringing of V_{DS1} and V_{DS2} between 50 MHz and 70 MHz in CIR 1. Therefore, as shown in Fig. 13(b), radiated EMI increases at that frequency. In particular, there is 80 dB of radiated EMI at 70 MHz. However, compared to the 72MHz peak of the conventional circuit, it is reduced by about 8dB. The radiated EMI at 112MHz is caused by the ringing at 120MHz in Fig. 12(b). However as shown in Fig. 11, about 60dB radiated EMI at 112MHz comes from the experimental equipment. Radiated EMI at this frequency from CIR 1 itself is at low level.

3) *Circuit proposed in previous research paper (CIR 2)*: As shown in Fig. 12(c), V_{DS2} waveform of CIR 2 has large ringing at 100 MHz when S2 is turned on. This 100 MHz ringing is a source of the 100 MHz radiated EMI in Fig. 13(c). In addition, 196 MHz and 290 MHz harmonics are generated from this 100 MHz radiated EMI. In CIR 1, the 120 MHz ringing in V_{DS2} occurs when S2 is turned on. However the radiated EMI of CIR 1 does not have a over 80 dB peak around 100 MHz

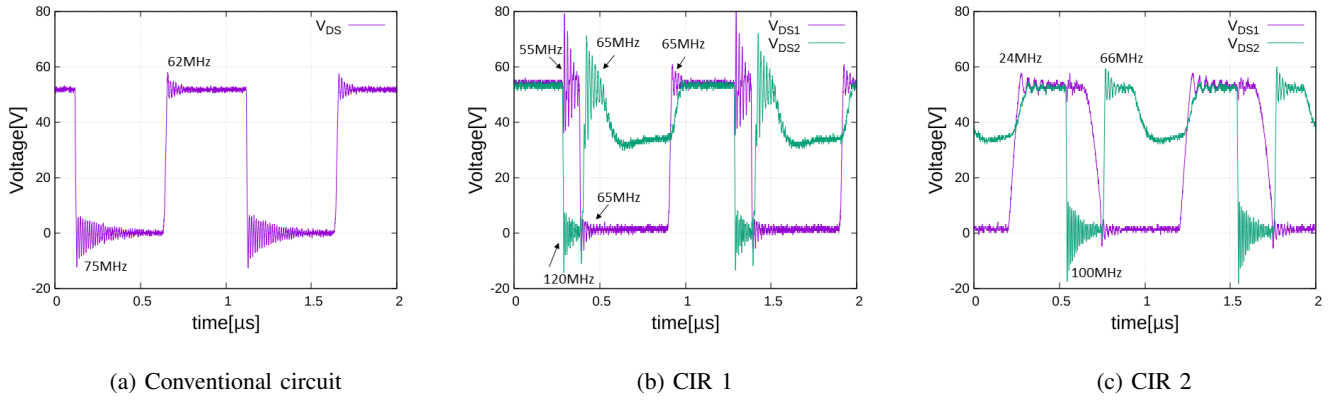


Fig. 12: Measurement results of V_{DS}

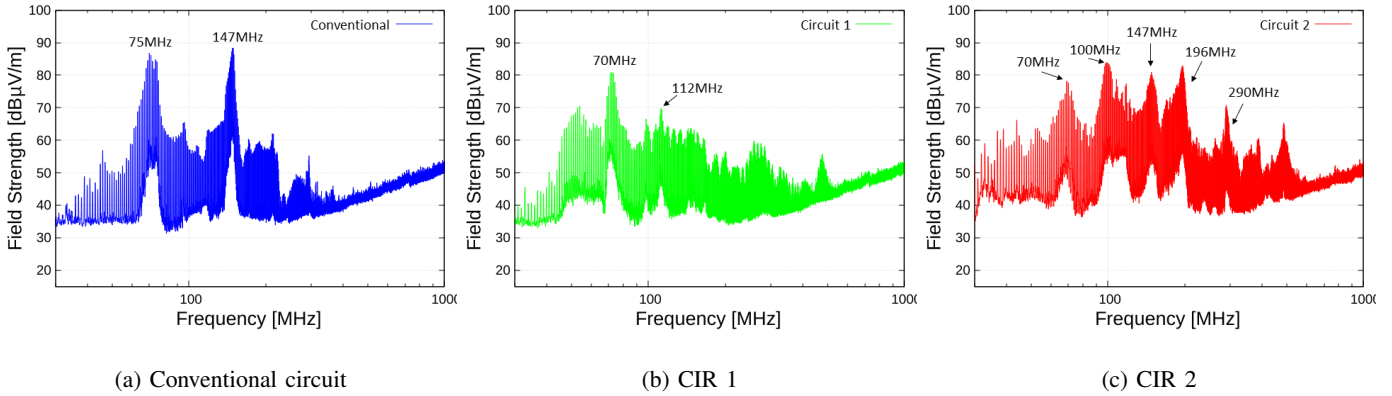


Fig. 13: Measurement results of radiated EMI

unlike that of CIR 2. In CIR 2, the longer on time of S2 than in CIR 1, and the longer time of ringing is considered to be the cause of the increase in radiated EMI above 100 MHz.

B. Efficiency

Figure 14 shows measurements results of conversion efficiency for each circuit. The conventional circuit is most efficient. Especially when output power is low, the difference between the conventional circuit and other circuits is significant. Efficiencies of CIR 1 and CIR 2 go down because their additional components increase conduction loss. When the output power is low, the efficiency is susceptible to conduction losses. Compared to efficiencies of CIR 1 and the conventional circuit, difference in efficiency is about 2.4% at output power of 100W, however, at an output power of 300W, the difference is decreased to about 1.0%.

Due to the same reason, efficiency of CIR 1 is higher than that of CIR 2. S2 of CIR 2 need longer on time than that of CIR 1 to discharge C1. It cause increasing conduction losses at L2, D2, S2 and D3. CIR 1 was more efficient than CIR 2 at all output power.

IV. CONCLUSION

In this paper, a boost dc-dc converter with turn on ZCS capability (CIR 1) is proposed in order to reduce radiated

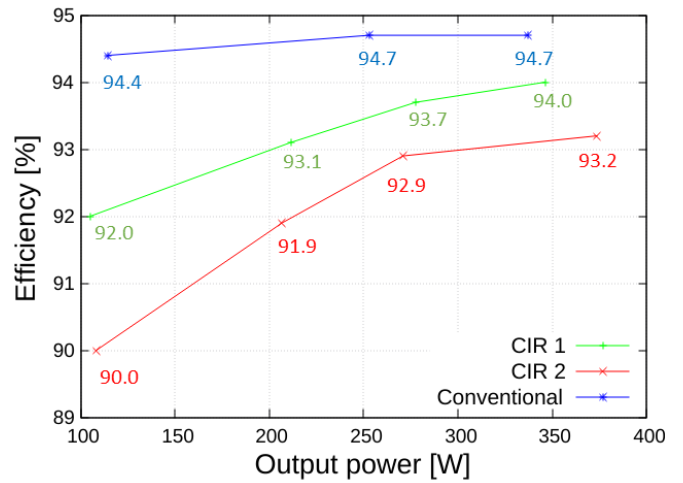


Fig. 14: Measurement results of efficiency

EMI The proposed circuit reduces radiated EMI at 70MHz by 7 dB caused by SiC-SBD reverse recovery current. Additionally, compared to the conventional circuit, the proposed circuit reduces radiated EMI at 140MHz coming from higher harmonics from radiated EMI due to SiC-SBD. However the

conversion efficiency is dropped by about 1%, because of conduction losses in additional components.

Compared to the circuit (CIR 2) proposed in the previous research paper [14], the proposed circuit (CIR 1) reduces radiated EMI above 100MHz. The efficiency of the proposed circuit is improved by 0.8% when output power is 350 W. We plan to improve efficiency by optimize circuit components, and measure at larger output power.

REFERENCES

- [1] F. Gamand, M. D. Li, and C. Gaquiere, "A 10-mhz gan hemt dc/dc boost converter for power amplifier applications," *IEEE Transactions on Circuits and Systems II: Express Briefs*, vol. 59, no. 11, pp. 776–779, 2012.
- [2] Y. Wu, M. Jacob-Mitos, M. L. Moore, and S. Heikman, "A 97.8gan hemt boost converter with 300-w output power at 1 mhz," *IEEE Electron Device Letters*, vol. 29, no. 8, pp. 824–826, 2008.
- [3] M. Abbasi, N. Mortazavi, and A. Rahmati, "A novel zvs interleaved boost converter," in *The 5th Annual International Power Electronics, Drive Systems and Technologies Conference (PEDSTC 2014)*, 2014, pp. 535–538.
- [4] Jing Xue, K. D. T. Ngo, and Hoi Lee, "A 99zero-voltage-switching boost converter using normally-off gan power transistors and adaptive dead-time controlled gate drivers," in *2013 IEEE International Conference of Electron Devices and Solid-state Circuits*, 2013, pp. 1–2.
- [5] J. Kwon, W. Choi, and B. Kwon, "Cost-effective boost converter with reverse-recovery reduction and power factor correction," *IEEE Transactions on Industrial Electronics*, vol. 55, no. 1, pp. 471–473, 2008.
- [6] W. Martinez, M. Noah, M. Yamamoto, and J. Imaoka, "Reverse-recovery current reduction in a zcs boost converter with saturable inductors using nanocrystalline core materials," in *2016 18th European Conference on Power Electronics and Applications (EPE'16 ECCE Europe)*, 2016, pp. 1–9.
- [7] M. Adamowicz, S. Giziewski, J. Pietryka, and Z. Krzeminski, "Performance comparison of sic schottky diodes and silicon ultra fast recovery diodes," in *2011 7th International Conference-Workshop Compatibility and Power Electronics (CPE)*, 2011, pp. 144–149.
- [8] G. Spiazzi, S. Buso, M. Citron, M. Corradin, and R. Pierobon, "Performance evaluation of a schottky sic power diode in a boost pfc application," *IEEE Transactions on Power Electronics*, vol. 18, no. 6, pp. 1249–1253, 2003.
- [9] P. Bog 垠 nez-Franco and J. B. Sendra, "Emi comparison between si and sic technology in a boost converter," in *International Symposium on Electromagnetic Compatibility - EMC EUROPE*, 2012, pp. 1–4.
- [10] D. Han, S. Li, W. Lee, W. Choi, and B. Sarlioglu, "Trade-off between switching loss and common mode emi generation of gan devices-analysis and solution," in *2017 IEEE Applied Power Electronics Conference and Exposition (APEC)*, 2017, pp. 843–847.
- [11] S. R. Holm, J. A. Ferreira, and P. R. Willcock, "Soft switching technique for lowering conducted emi on a three phase boost converter," in *PESC 98 Record. 29th Annual IEEE Power Electronics Specialists Conference (Cat. No.98CH36196)*, vol. 1, 1998, pp. 865–870 vol.1.
- [12] S. Rahmani, M. Mohammadi, and M. R. Yazdani, "Emi prediction of a new zct two-switch flyback converter," in *2014 22nd Iranian Conference on Electrical Engineering (ICEE)*, 2014, pp. 322–327.
- [13] D.-K. Kwak, "A new boost dc-dc converter of high efficiency by using a partial resonant circuit," *IEICE Electronics Express*, vol. 6, no. 12, pp. 844–850, 2009.
- [14] Guichao Hua, Ching-Shan Leu, Yimin Jiang, and F. C. Y. Lee, "Novel zero-voltage-transition pwm converters," *IEEE Transactions on Power Electronics*, vol. 9, no. 2, pp. 213–219, 1994.
- [15] P. Sojka, M. Pipiska, and M. Frivaldsky, "Gan power transistor switching performance in hard-switching and soft-switching modes," in *2019 20th International Scientific Conference on Electric Power Engineering (EPE)*, 2019, pp. 1–5.